Variable In Situ Stress Orientations Across the Northern Hikurangi Subduction Margin

D. D. McNamara[1] , E. Behboudi[2] , L. Wallace[3,4] , D. Saffer[4], A. E. Cook[5] , A. Fagereng[6] , M. Paganoni[7], Hung-Yu Wu[8], G. Kim[9], H. Lee[9], H. M. Savage[10] , P. Barnes[11] , I. Pecher[12] , L. J. LeVay[13] , and K. E. Petronotis[13]

[1]Department of Earth, Ocean and Ecological Sciences, University of Liverpool, Liverpool, UK, [2]Irish Centre for Research in Applied Geoscience, University College Dublin, Dublin, Ireland, [3]GNS Science, Lower Hutt, New Zealand, [4]University of Texas Institute for Geophysics, Austin, TX, USA, [5]School of Earth Sciences, Ohio State University, Columbus, OH, USA, [6]School of Earth and Environmental Sciences, Cardiff University, Cardiff, UK, [7]Department of Earth Science, University of Oxford, Oxford, UK, [8]Department of Resources Engineering, National Cheng Kung University, Tainan, Taiwan, [9]Korea Institute of Geoscience and Mineral Resources (KIGAM), Daejeon, Korea, [10]Department of Earth and Planetary Sciences, University of California, Santa Cruz, Santa Cruz, CA, USA, [11]National Institute of Water and Atmospheric Research (NIWA), Wellington, New Zealand, [12]School of Environmental and Marine Sciences, University of Auckland, Auckland, New Zealand, [13]International Ocean Discovery Program, Texas A&M University, College Station, TX, USA

Abstract We constrain orientations of the horizontal stress field from borehole image data in a transect across the Hikurangi Subduction Margin. This region experiences NW-SE convergence and is the site of recurrent slow slip events. The direction of the horizontal maximum stress is E-W at an active splay thrust fault near the subduction margin trench. This trend changes to NNW-SSE in a forearc trench slope basin on the offshore accretionary wedge, and to NE-SW in the onshore forearc. Multiple, tectonic, and geological processes, either individually or in concert, may explain this variability. The observed offshore to onshore stress rotation may reflect a change from dominantly compressional tectonics at the deformation front, to a strike-slip and/or extensional tectonic regime closer to the Taupo Volcanic Zone, further inland. In addition, the offshore stress may be affected by topography and/or stress rotation around subducting seamounts, and/or temporal stress changes during the slow slip cycle.

Plain Language Summary Using geophysical images captured from the inside of boreholes drilled across the Hikurangi Subduction Margin, an area that experiences slow earthquakes, we describe variability in the direction of modern day maximum horizontal tectonic forces (stress) at this collisional plate boundary. Changes in the direction of maximum horizontal stress occur as you move from the plate boundary toward the onshore region of New Zealand's North Island. We suggest a range of possible tectonic and geological processes that either individually or in concert may explain our observed stress direction variations. This includes changing tectonic regimes as you move away from the plate boundary, topography, and effects on the stress field caused by the presence of subducting seamounts, and changing stress conditions related to the intermittent activity of slow earthquakes.

1. Introduction

The stress state in the crust exerts a fundamental control on crustal deformation, earthquake dynamics, the generation and maintenance of topography, and crustal hydrology (Duan, 2010; Ito & Zoback, 2000; Miller & Dunne, 1996; Sibson et al., 2011; Warren-Smith et al., 2019; M. D. Zoback & Townend, 2001). Fault slip resulting from stress accumulation is a function of the orientation and magnitudes of the three principal stresses ($\sigma_1 > \sigma_2 > \sigma_3$), subsurface pore pressures (P_p), existing fault orientations, and rock cohesion and friction (Anderson, 1906; M. L. Zoback et al., 1989). Stress orientations, magnitudes, and P_p can in turn be altered by local topography, mechanical contrasts of subsurface geological units, and earthquake and creep activity. Studies of active tectonic systems, including shallow subduction zones, reveal both temporal and spatial perturbations in the crustal stress state related to fault geometry and activity (Byrne et al., 2009; Chang et al., 2010; Hardebeck & Okada, 2018; Lin et al., 2009; McNamara et al., 2015), earthquake slip

(Allmann & Shearer, 2009; Brodsky et al., 2017; Lin et al., 2013, 2015), and redistribution of pore pressure (Magee & Zoback, 1993; Song et al., 2011).

Episodic, shallow (<15 km) slow slip events (SSE), spanning timescales ranging from days to years, are recorded at several subduction zones, including the Nankai margin, offshore Japan (Araki et al., 2017; Hirose et al., 1999; Obara et al., 2004), the Costa Rican margin (Davis et al., 2015; Dixon et al., 2014), and the Hikurangi Subduction Margin (HSM) (Wallace et al., 2012, 2016). Despite the recognized importance of stress in earthquake dynamics, data constraining stress states and variability on, and in the near field of, faults that host SSEs is limited (Chang et al., 2010; Huffman et al., 2016; Warren-Smith et al., 2019). This study provides new data on contemporary stress orientation variability across an area of recurring slow slip in the northern HSM. We characterize shallow crustal stress orientations from boreholes along a transect from the actively deforming frontal accretionary wedge, through the landward, offshore Tuaheni Basin (a forearc trench slope basin), and onto the onshore forearc (Figure 1). We then discuss possible geological processes responsible for the observed stress orientation variations.

1.1. State of Stress at the Hikurangi Subduction Margin

The HSM accommodates westward subduction of the Pacific plate beneath the North Island of New Zealand at rates of ∼2–3 cm/year in the south, and ∼6 cm/year in the north (Figure 1a) (Wallace et al., 2004). Northward convergence rate increase at the trench is due to forearc clockwise rotation, which also creates changes in upper plate tectonics along-strike of the margin. Pacific-Australia plate convergence is oblique, with the margin-perpendicular component accommodated primarily along shallow subduction thrust faults, and the margin-parallel component accommodated by a combination of forearc rotation and strike-slip in the onshore North Island Dextral Fault Belt (Beanland & Haines, 1998; Wallace et al., 2004). Episodic SSEs are observed at shallow depths of 2–15 km at the northern HSM every 1–2 years, and involve ≤20 cm of slip on the plate boundary occurring over a few weeks (Wallace et al., 2010, 2016). There have also been moderate-sized subduction thrust earthquakes in the north Hikurangi SSE source region, including two M_w 7.0–7.2 events in 1947 (Figures 1b and 1c) (Doser & Webb, 2003).

Aspects of the HSM stress state have been reported previously. In the onshore northern HSM, focal mechanism-derived S_{Hmax} directions are NE-SW (oblique to relative plate motion, and approximately parallel to HSM margin strike), with suggested local variation to ENE-WSW S_{Hmax} orientations in the area east of Gisborne (subparallel to relative plate motion, and HSM strike-oblique) (Townend et al., 2012). Borehole image logs (acquired within the upper 3 km of the crust) from three onshore wells (Kauhauroa-2, Kauhauroa-5, and Tuhara-1A) also show NE-SW S_{Hmax} orientations in the Hawke's Bay region (Lawrence, 2018). Investigations of the principal contraction (strain) direction from GPS measurements along the HSM are highly variable, with dominantly east-west directions near the east coast, and with some rotation to NE-SW further inland (Dimitrova et al., 2016; Haines & Wallace, 2020).

P_p measured from drill stem tests and repeat formation testing, and inferred from mud weights in onshore wells, reveal shallow overpressures within basins of the upper plate (Burgreen-Chan et al., 2016; Darby & Funnell, 2001). The southern Wairarapa and south Hawke's Bay regions display lower overpressures than the northern Raukumara and north Hawke's Bay regions of the northern HSM. Overpressures are found within Cretaceous-Paleogene, smectite-rich seal rocks of the Wanstead Formation, are spatially variable within Neogene, low-permeability, mudstone units, and are uncommon within Quaternary units (Darby & Funnell, 2001). These shallow overpressures have been attributed to both disequilibrium compaction, where pore water flow is restricted during sediment compaction, and to porosity reduction associated with high horizontal compressive stresses related to plate convergence (Burgreen-Chan et al., 2016; Darby & Funnell, 2001). Finally, in the Hawke's Bay region, σ_3 magnitudes determined from leak-off tests performed in onshore wells are less than (though in places close to) vertical stress (S_v) magnitudes, suggesting that normal, strike-slip, and potentially reverse faulting stress regimes are experienced here (Burgreen-Chan et al., 2016).
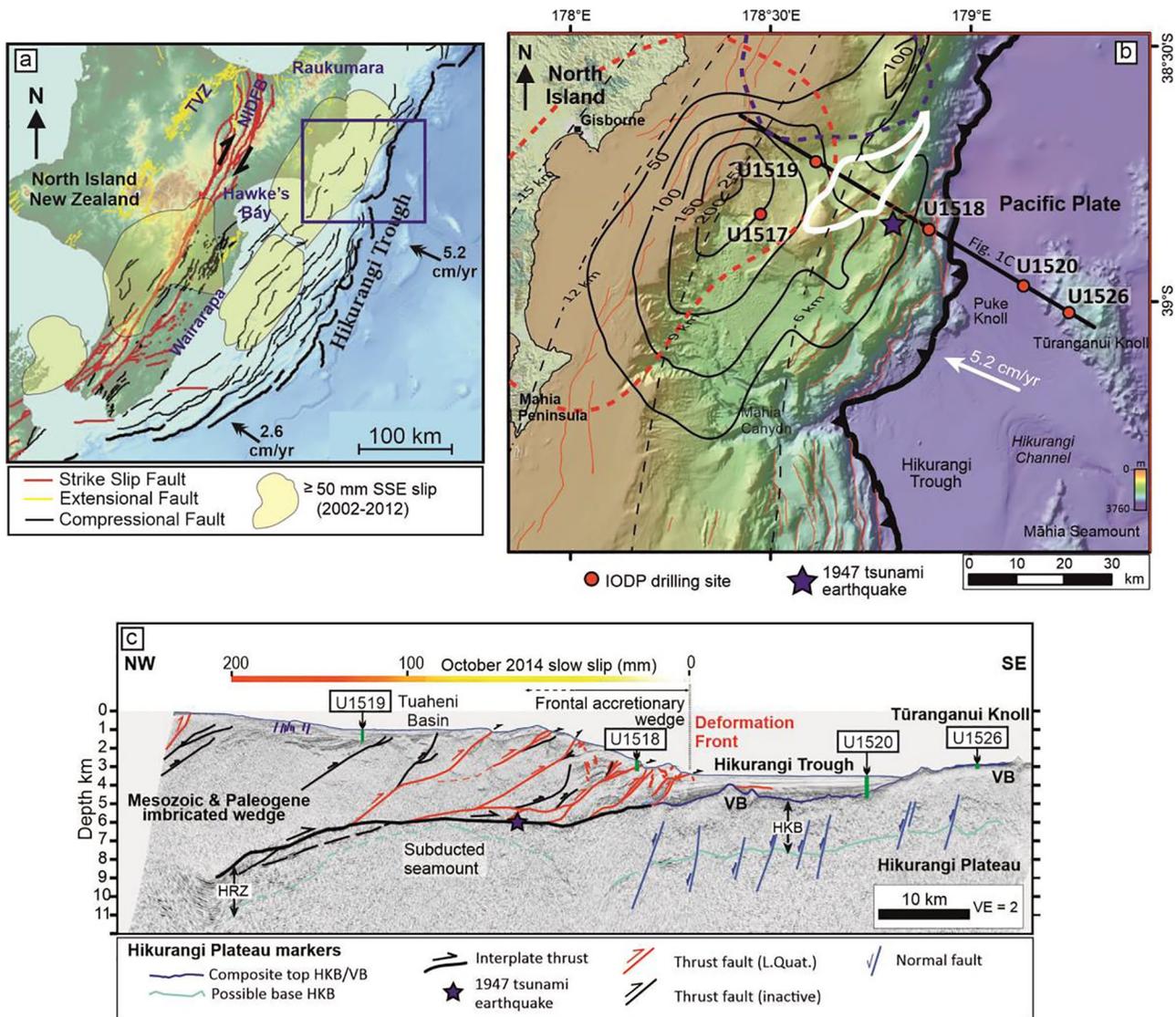
Figure 1. (a) Map of the North Island of New Zealand, tectonic structures, and regions that have experienced cumulative slow slip of ≥50 mm between 2002 and 2012 (Wallace & Eberhart-Phillips, 2013). Fault traces from Barnes et al. (2010); Langridge et al. (2016); Mountjoy and Barnes (2011); Pedley et al. (2010); blue square is the area depicted in Figure 1b. TVZ, Taupo Volcanic Zone. (b) Bathymetric map showing the IODP Expeditions 372 and 375 drill Sites (U1517, U1519, U1518, U1520, and U1526), and seismic line 05CM-04 (black line). Modified from Barnes et al. (2020), the figure shows the extent of three recent SSEs (fine black lines with labels are slip contours (mm) for the September–October 2014 SSE, the blue dashed line is the 40-mm slip contours for the January–February 2010 SSE, and the red dashed line is the 40-mm slip contour for the March–April 2010 SSE (Wallace et al., 2016), dashed black lines show approximate depths of the plate interface (Williams et al., 2013), bold black line with teeth marks = plate boundary deformation front, fine red lines = upper plate thrust fault traces, bold white line = approximate morphology of an inferred subducted seamount (Barker et al., 2018). (c) Interpretation of NW-SE seismic profile 05CM-04 (modified from Barnes et al. [2020]), showing interpreted location of major structures, and well locations (green lines). Colored scale shows amount of slip across the HSM during the 2014 SSE (Wallace et al., 2016), HKB, Hikurangi Basement, VB, Volcanic Basement.

2. Methods and Data

2.1. GVR Resistivity Image Log Processing and Analysis

International Ocean Discovery Program (IODP) Expeditions 372/375 drilled a series of wells across the HSM (Wallace et al., 2019b) (Figure 1). During Expedition 372, a suite of LWD data, including geoVISION (GVR) resistivity image logs, were acquired in Holes U1517A, U1518A/B, U1519A, and U1520A/B. Hole U1517A was drilled through bedded, clayey-silt sediment packages associated with the Tuaheni Landslide Complex (Pecher et al., 2019). Hole U1518A/B drilled across the Pāpaku Fault, an active splay thrust in the

frontal accretionary wedge, and the bedded sediments that comprise its hangingwall and footwall (Fagereng et al., 2019; Saffer et al., 2019). Hole U1519A is located within an upper continental slope sedimentary basin (Tuaheni Basin) and intersects bedded mudstones, siltstones, and sandstone packages, as well as mass transport deposits (Barnes et al., 2019). Finally, Hole U1520A/B is located on the incoming subducting plate and intersects trench-wedge clastic sediments and a lower sequence of carbonates and volcaniclastics (Barnes et al., 2020).

GVR resistivity image logs are analyzed in this study to identify and quantify the properties of stress-induced borehole features such as borehole breakouts. GVR logging uses rotating resistivity buttons to provide a 360° resistivity image of the borehole wall. This study reports borehole breakout orientation results determined from a high-resolution, post-expedition reanalysis of the GVR image logs which has resulted in a more detailed and accurate data set than the preliminary data provided from the shipboard analysis (Wallace et al., 2019b). Raw data was processed from the GVR tool following the procedure detailed in Wallace et al. (2019a). For this study, all GVR images (those generated from the shallow, medium, and deep resistivity button) were analyzed. The shallow button GVR image logs are the preferred image for data acquisition as they have a higher potential of recording features close to the borehole wall, including stress-induced features. The GVR image logs were statically and dynamically normalized to enhance resistivity contrasts for improved feature identification, with a 1 and 0.5 m normalization window used for the latter. Feature classification is based on criteria set out in McNamara et al. (2019). Quality rankings and circular statistics for stress induced borehole features identified from the GVR image logs follow World Stress Map criteria (Heidbach, 2016).

3. Results

3.1. Borehole Image Stress-Induced Features

From all GVR image logs collected during IODP Expedition 372, 86 distinct borehole breakout pairs are identified in Holes U1518A/B and U1519A (Table 1; Figure 2); none were identified within other Holes. No drilling-induced tensile fractures, or petal centerline fractures are observed on any GVR image logs. Borehole breakouts, were observed, are more common at deeper depths. No systematic correlation between the occurrence of borehole breakouts and well logging units is confidently observed. Individual borehole breakouts are observed to cross multiple individual bedding layers in both U1518 and U1519 Holes.

Borehole breakout azimuths are variable between the two drillsites and with depth in each individual Hole (Figure 2). Stress indicator quality ranking for both holes is "D" meaning the stress orientations observed are likely more representative of local stress states than regional stress states (Tingay et al., 2008). Eight of the 10 borehole breakout pairs identified in Hole U1518 occur between 518 and 591 mbsf (meters below seafloor) and have an average orientation of 003° ± 6°/180° ± 4° (Figure 2a). These lie in the footwall of the Pāpaku fault that was intersected at 315–348 mbsf (Cook et al., 2020). From these breakout orientations, we report an $S_{h\min}$ orientation of N-S, and infer an $S_{H\max}$ orientation of E-W (Figures 2a and 2b). Orientation trend variations between borehole breakouts <10 m apart ranges from 3° to 16° within this interval (Figure 2a). In the hanging wall (~210–220 mbsf), two borehole breakout pairs (low resistivity zones, ~180° apart around the borehole, associated with increased caliper values) are identified and have 065°/252° and 056°/236° azimuths (Figure 2a), from which a NE-SW $S_{h\min}$ and NW-SE $S_{H\max}$ orientation is inferred.

At Hole U1519A, 72 borehole breakout pairs have average azimuths of 072° ± 13°/252° ± 9° (Table 1), corresponding to an ENE-WSW $S_{h\min}$ and NNW-SSE $S_{H\max}$ orientation (Figures 2c and 2d). Most borehole breakouts cluster within two depth intervals, 585–605 mbsf (cluster A) and 630–650 mbsf (cluster B) (Figure 2c). Localized variation of borehole breakout azimuth (between borehole breakouts <10 m apart) ranges from <1° to 52° (average of 12° ± 9°) (Figure 2c). The largest of these azimuth variations (52°) occurs at ~545 mbsf though this includes a borehole breakout azimuth (029°) that sits outside the circular statistical range for Hole U1519A the formation of which may not accurately reflect the stress orientation (Figure 2c). Both clusters show a maximum borehole breakout azimuth variation of 31° at 607.5 mbsf (cluster A) and 658.5 mbsf (cluster B).

Table 1
Stress Indicators From Analyzed LWD Resistivity Image From IODP Expedition 372

Hole	U1518B	U1519A
Latitude	38°51.5476'S	38°43.6372'S
Longitude	178°53.7621'E	178°36.8537'E
Average borehole breakout azimuth (°)	003/180[a]	072/252
S.D. (°)	4/6[a]	9/13
Feature type	Borehole breakout	Borehole breakout
N	10	76
Total length of borehole breakouts (m)	2.2	16.9–17.3
Stress indicator quality ranking	D	D
Date of image logging	December 21, 2017	December 24, 2017
Top borehole breakout depth (mbsf/mrsl)	210/2,844	17/1,028
Bottom borehole breakout depth (mbsf/mrsl)	591/3,225	650/1,662
Sea floor depth (mrsl)	2634.6	1000.7
Distance between rig floor and sea level (m)	10.9	10.9
Image log top (mbsf/mrsl)	54.5/2,689.1	12/1024.2
Image log bottom (mbsf/mrsl)	647.1/3281.7	755.8/1756.5
Well orientation	Vertical	Vertical

Note. Average borehole breakout azimuths and standard deviations (S.D.) calculated according to World Stress Map criteria (Mardia, 1975; Tingay et al., 2008) and show values generated for both pairs of borehole breakout sets. N = number of borehole breakout pairs. Stress indicator quality ranking determined from Tingay et al. (2008). mrsl, meters relative to sea level; mbsf, meters below seafloor.

[a]Average and standard deviation values for Hole U1518B are calculated from the eight borehole breakouts observed in the Pāpaku fault footwall due to low confidence in the two observed in the hangingwall.

4. Discussion

The stress orientation data presented here are the first direct measurements made across the offshore northern HSM (Figure 3). At the borehole scale, S_{Hmax} rotates from an E-W orientation at the Pāpaku fault, an active splay thrust fault near the deformation front (Site U1518), to a NNW-SSE orientation above the plate interface where peak slip in SSEs occurs (Site U1519), and finally to a NE-SW orientation in onshore wells (Figure 3). Recent investigation of seismic anisotropy across this HSM offshore region shows fast azimuths align with observed U1518 and U1519 borehole-derived S_{Hmax} orientations (Arai et al., 2020; Zal et al., 2020). Geological and tectonic influences on stress direction variability at both the well scale and across the northern HSM are discussed here.

4.1. Well-Scale Stress Orientation Variability at Sites U1518 and U1519

The rotation of S_{Hmax} within Hole U1518B from NW-SE direction in the Pāpaku Fault hanging wall to E-W in the footwall is indicated by a small number of data points. This depth-related stress rotation, if real, may be explained by a number of processes acting in combination or separately. First, as the Pāpaku Fault is an active splay fault near the trench, recent slip on this structure may have perturbed the stress field. Second, the NW-SE S_{Hmax} orientation is observed within a depth interval of core-scale hanging wall folds and fractures (Fagereng et al., 2019). LWD resistivity image logs of this same depth interval also reveal the presence of fracturing and bedding orientation patterns consistent with large-scale folding (Saffer et al., 2019). Recent slip on faults and fractures associated with this deformed depth interval may have generated a local rotation on the stress directions in this region. Third, east of Hole U1518B, there is an abrupt change in topography which may influence the formation and orientation of the shallower stress-induced wellbore failures observed here (Figure 1c; M. L. Zoback et al., 1989). This topography may also have a broader effect on the overall observed E-W S_{Hmax} orientation observed at Site U1518. Modeling of the spatial influence of the
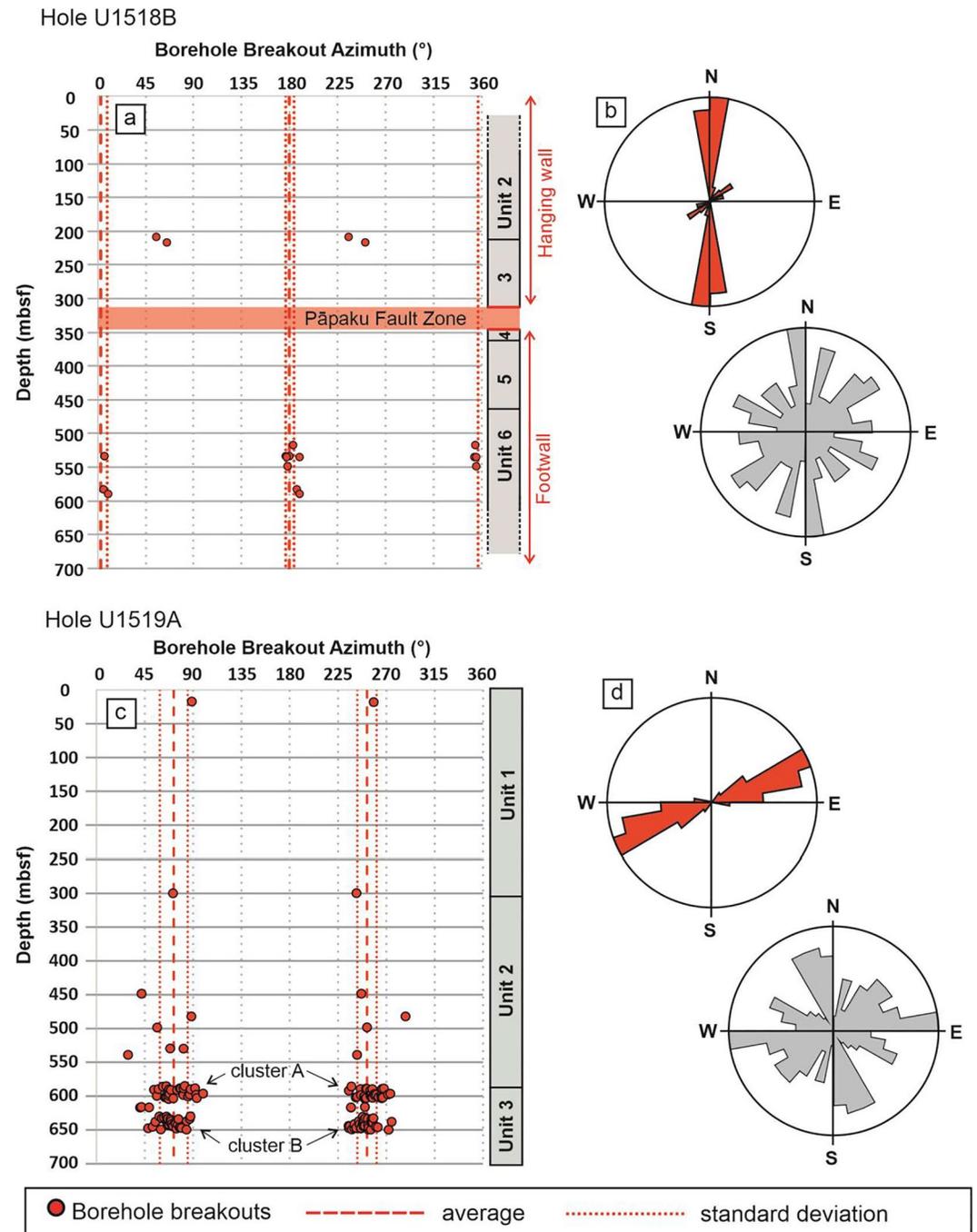
Figure 2. (a) Borehole breakout azimuth as a function of depth (mbsf) in Hole U1518B. Depth extent of the Pāpaku Fault and LWD-defined units shown on the right (Cook et al., 2020; Saffer et al., 2019). (b) Bi-directional rose diagrams of Hole U1518B borehole breakout azimuths (red) and structural strikes (gray). (c) Borehole breakout azimuth in Hole U1519A as a function of depth (mbsf). LWD-defined units shown on the right (Barnes et al., 2019). (d) Bi-directional rose diagrams of Hole U1519A borehole breakout azimuths (red) and structural strikes (gray).

topographical feature on local stress conditions at Site U1518, and more than two borehole breakout measurements are required in this region to confirm and explain the causes of stress rotations with depth here.

The small-scale variation in borehole breakout orientation within Hole U1519A is likely due to stress field perturbation from localized deformation in these depth intervals. This is supported by the large number of
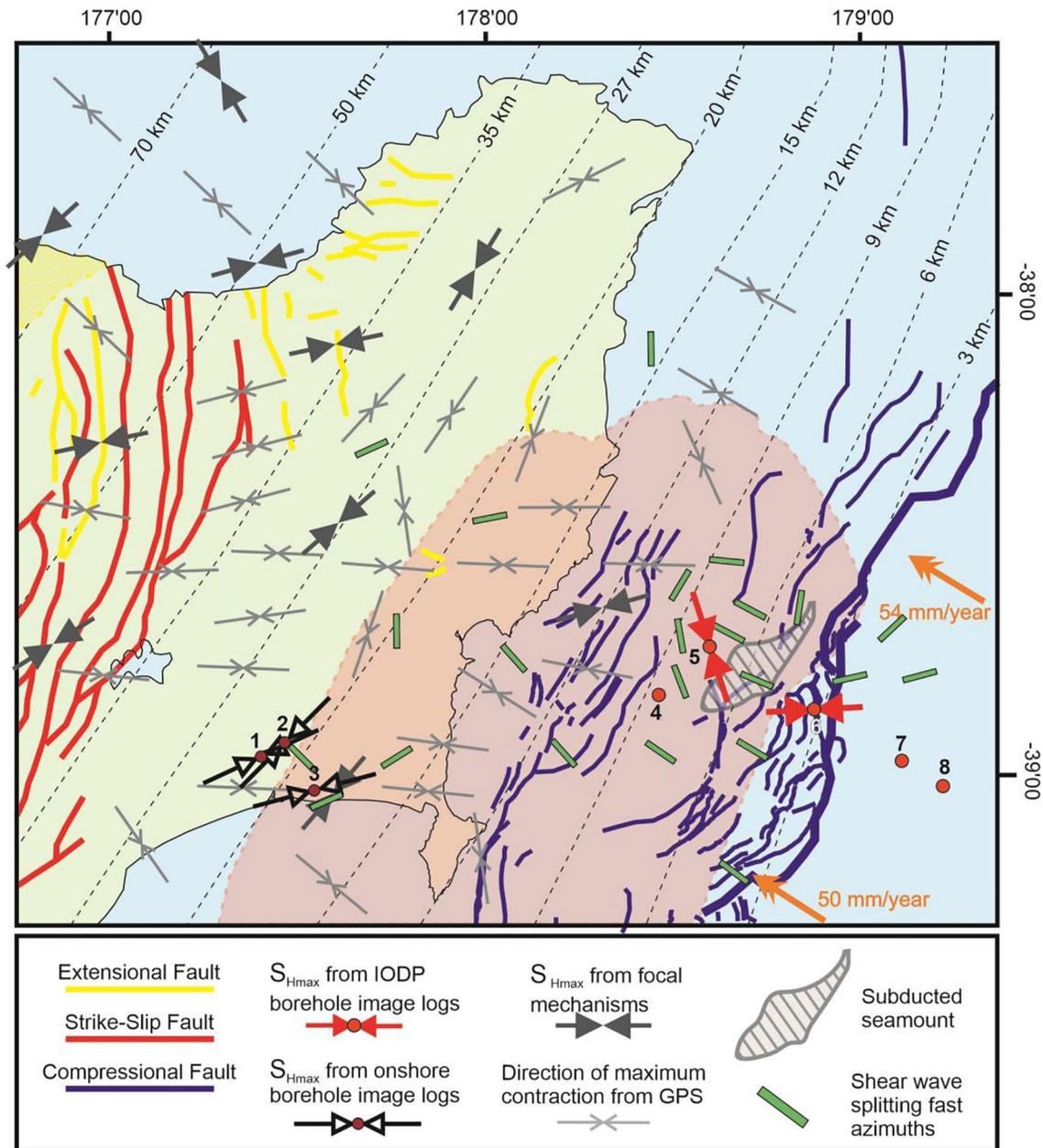
Figure 3. Map of the northern HSM showing S_{Hmax} orientations from IODP borehole image logs, onshore borehole image analysis from Lawrence (2018), and focal mechanism S_{Hmax} from Townend et al. (2012). Also shown is the direction of maximum contraction from GPS (Haines & Wallace, 2020) and green bars show selected average shear wave splitting fast azimuths (Zal et al., 2020). Plate convergence direction (orange arrows) and rate obtained from Wallace et al. (2012). Wells are numbered (1 – Kauhauroa-2, 2 – Kauhauroa-5, 3 – Tuhara-1A, 4 – U1517, 5 – U1519A, 6 – U1518B, 7 – U1520B, 8 – U1526). Thin, dashed, black lines show depth contours to the subduction interface (Williams et al., 2013), and the transparent red zone is the extent of cumulative slow slip in the northern HSM occurring between 2002 and 2012 (Wallace et al., 2012). Faults traces from Barnes et al. (2010); Langridge et al. (2016); Mountjoy and Barnes (2011); Pedley et al. (2010).

fractures and observation of deformed bedding within these depth intervals, as noted from LWD resistivity borehole imaging (Barnes et al., 2019).

4.2. Stress Orientation Variability Across the Northern HSM

A number of geological and tectonic phenomena, either in isolation or in concert, could explain the observed S_{Hmax} orientation variability across the northern HSM, from the trench through to the onshore

forearc. The E-W $S_{H\max}$ in the Pāpaku fault footwall (Site U1518), is consistent with the location of this site in a region characterized by horizontal compression subparallel to relative plate convergence. An E-W $S_{H\max}$ orientation is further supported by the N-S strike of thrust splay faults imaged in seismic and bathymetric data from this area (Barker et al., 2018; Barnes et al., 2020), and E-W shortening directions inferred from sediment magnetic susceptibility anisotropy measured from the Pāpaku Fault footwall (Greve et al., 2020).

NNW-SSE orientations reported from Hole U1519A are not aligned with NE-SW $S_{H\max}$ (margin parallel) orientations reported from onshore wells and derived from focal mechanisms, nor with E-W $S_{H\max}$ orientations reported from Hole U1518B (Figure 3). Several factors may explain this discrepancy. First, Hole U1519A is located ∼5 km above a zone of the plate interface that experiences regular large SSEs, and is locked in-between these events (Wallace et al., 2010, 2016) (Figure 1c). Hole U1519A was drilled and logged during a time in-between SSEs, when the subduction plate interface was locked, and elastic strain accumulation was occurring, similar to past inter-SSE periods (Wallace et al., 2010). As stress orientations from existing onshore industry wells are located above the steadily creeping plate interface region (with no locking and minimal slow slip; Figures 1 and 3), the observed difference in $S_{H\max}$ orientations may be related to differences in plate interface behavior (creeping beneath the onshore region; locking and episodic SSEs offshore). This assumes that stress states at the plate interface remain broadly consistent from the plate interface depth to shallow crustal levels. We also note that the broadly NE-SW orientation of the onshore $S_{H\max}$ observations may also be related to the position of the northern Hikurangi forearc to the east of an actively extending intra-arc rift (the TVZ). Here, the forearc is likely to be under margin-normal (southeast-directed) extension, due to the transmission of slab rollback forces across the forearc and into the extending arc region (Wallace et al., 2012).

The observed NNW-SSE $S_{H\max}$ orientation at Hole U1519A may also result from the influence of a subducting seamount which has been inferred between Sites U1519 and U1518 (Barker et al., 2018). It has been inferred that observed fast azimuth directions around this seamount are likely related to effect the subducting seamount has on local structure and stress patterns (Arai et al., 2020; Zal et al., 2020). Numerical modeling suggests that enhanced lateral compression ($S_{H\max}$ magnitude), rotation of $S_{H\max}$, and increased fault-normal stresses can be expected ahead of the landward flank of the subducting seamount, while creating an extensional stress shadow behind it (Sun et al., 2020). Given that Hole U1519A is located on the landward side of the proposed subducting seamount, and in the context of the approximate seamount morphology that is elongate parallel to the margin (NE-SW), this may explain the observed NNW-SSE compressional direction of $S_{H\max}$ here (Figure 3). This theory, however, would require a morphological feature at the plate interface to generate a perturbation large enough to affect the stress field at shallow levels where borehole breakouts are being measured. Furthermore, this effect would have to only apply to the leading flank and not the extensional stress shadow, in order to explain the compressional $S_{H\max}$ orientation at Site U1518 (which is located seaward of the seamount, in the expected stress shadow).

The borehole breakout-derived $S_{H\max}$ orientations recorded from Hole U1519A may represent a transient stress state associated with the current interseismic SSE period, which may change during SSE. If so, stress states during SSEs in this region could either rotate the $S_{H\max}$ orientation, change the stress state from compressional to strike-slip or extension as a result of the small, typically several to tens of kPa (Ikari et al., 2020), or allow a combination of both. Analysis of fracture orientations from GVR image logging at Site U1519 (Data Set 2) shows a dominant NNE-SSW strike consistent with the interseismic NNW-SSE compressional $S_{H\max}$ direction, though multiple strike orientations seen for subordinate fractures may be more consistent with alternative stress states to the one observed at the time of drilling. These may reflect temporal rotations in $S_{H\max}$ orientation. If SSE stress drops reduce $S_{H\max}$ below the S_V magnitude, becoming σ_2 to create an extensional stress state, then from calculated total S_v magnitudes of the region (Data Set 1), the interseismic $S_{H\max}$ magnitude would fall in the region of ∼19–28 MPa. Until stress orientations can be quantified during SSE, further fracture orientation analysis is performed, and/or quantification of the interseismic $S_{H\max}$ magnitude from existing data is carried out, this idea remains conjectural, though worthy of further investigation.

Overall, offshore borehole breakout-derived $S_{H\max}$ orientations from IODP wells (NNW-SSE, and E-W) differ from the documented NE-SW $S_{H\max}$ for the northern HSM from shallow depths to plate interface (Lawrence, 2018; Townend et al., 2012). This likely reflects a transition from a thrust fault regime in

margin-normal compression at the northern HSM deformation front, to extensional (normal-faulting) and strike-slip tectonics in the onshore forearc of the northern HSM forearc, adjacent to the actively extending Taupo Volcanic Zone. We suggest that the offshore IODP stress orientations presented here are influenced by processes occurring near the deformation front, including topographical effects, possible temporal effects associated with the SSE cycle, and spatial effects associated with the presence of a subducting seamount in the region.

5. Conclusions

Changes in horizontal stress orientations are observed in a transect across the northern HSM. Borehole image log S_{Hmax} orientations imply margin-normal (E-W), maximum compression in the Pāpaku thrust fault footwall, a compressional NNE-SSW orientation in the forearc offshore Tuaheni Basin, and a NE-SW orientation consistent with strike-slip faulting further landward, within the onshore forearc. The NNW-SSE S_{Hmax} observed ~40 km east of the coast at Site U1519 may reflect a number of offshore subduction-related processes including temporal variations in subduction interface locking and elastic strain accumulation associated with the SSE cycle, and/or spatial controls associated with subducting seamounts in this region. Well-scale variations in stress orientation are likely caused by a combination of topographic effects and recent activity on active fractures and faults.

Data Availability Statement

This research used data provided by the International Ocean Discovery Program (IODP). The well data used in this paper can accessed through IODP's database (http://mlp.ldeo.columbia.edu/logdb/ scientific_ocean_drilling/).

References

Allmann, B. P., & Shearer, P. M. (2009). Global variations of stress drop for moderate to large earthquakes. *Journal of Geophysical Research*, *114*, B01310. https://doi.org/10.1029/2008jb005821

Anderson, E. M. (1906). The dynamics of faulting. *The Journal of Geology*, *14*(3), 254–257. https://doi.org/10.1086/621305

Arai, R., Kodaira, S., Henrys, S., Bangs, N., Obana, K., Fujie, G., et al. (2020). Three-dimensional P wave velocity structure of the Northern Hikurangi Margin from the NZ3D experiment: Evidence for fault-bound anisotropy. *Journal of Geophysical Research: Solid Earth*, *125*(12), e2020JB020433. https://doi.org/10.1029/2020jb020433

Araki, E., Saffer, D. M., Kopf, A. J., Wallace, L. M., Kimura, T., Machida, Y., et al. (2017). Recurring and triggered slow-slip events near the trench at the Nankai Trough subduction megathrust. *Science*, *356*(6343), 1157–1160. https://doi.org/10.1126/science.aan3120

Barker, D. H. N., Henrys, S., Tontini, F. C., Barnes, P. M., Bassett, D., Todd, E., & Wallace, L. (2018). Geophysical Constraints on the relationship between seamount subduction, slow slip, and tremor at the north Hikurangi subduction zone, New Zealand. *Geophysical Research Letters*, *45*(2), 12. https://doi.org/10.1029/2018gl080259

Barnes, P. M., Lamarche, G., Bialas, J., Henrys, S., Pecher, I., Netzeband, G. L., et al. (2010). Tectonic and geological framework for gas hydrates and cold seeps on the Hikurangi Subduction Margin, New Zealand. *Marine Geology*, *272*(1–4), 26–48. https://doi.org/10.1016/j.margeo.2009.03.012

Barnes, P. M., Wallace, L. M., Saffer, D. M., Bell, R. E., Underwood, M. B., Fagereng, A., et al. (2020). Slow slip source characterized by lithological and geometric heterogeneity. *Science Advances*, *6*(13), eaay3314. https://doi.org/10.1126/sciadv.aay3314

Barnes, P. M., Wallace, L. M., Saffer, D. M., Pecher, I. A., Petronotis, K. E., LeVay, L. J., et al. (2019). *Proceedings of the International Ocean Discovery Program Site U1519*. Undefined. https://doi.org/10.14379/iodp.proc.372b375.104.2019

Beanland, S., & Haines, J. (1998). The kinematics of active deformation in the North Island, New Zealand, determined from geological strain rates. *New Zealand Journal of Geology and Geophysics*, *41*(4), 311–323. https://doi.org/10.1080/00288306.1998.9514813

Brodsky, E. E., Saffer, D., Fulton, P., Chester, F., Conin, M., Huffman, K., et al. (2017). The postearthquake stress state on the Tohoku megathrust as constrained by reanalysis of the JFAST breakout data. *Geophysical Research Letters*, *44*(16), 8294–8302. https://doi.org/10.1002/2017gl074027

Burgreen-Chan, B., Meisling, K. E., & Graham, S. (2016). Basin and petroleum system modeling of the East Coast Basin, New Zealand: A test of overpressure scenarios in a convergent margin. *Basin Research*, *28*(4), 536–567. https://doi.org/10.1111/bre.12121

Byrne, T. B., Lin, W., Tsutsumi, A., Yamamoto, Y., Lewis, J. C., Kanagawa, K., et al. (2009). Anelastic strain recovery reveals extension across SW Japan subduction zone. *Geophysical Research Letters*, *36*, L23310. https://doi.org/10.1029/2009gl040749

Chang, C., McNeill, L. C., Moore, J. C., Lin, W., Conin, M., & Yamada, Y. (2010). In situ stress state in the Nankai accretionary wedge estimated from borehole wall failures. *Geochemistry*, *11*(1), Q0AD04. https://doi.org/10.1029/2010gc003261

Cook, A. E., Paganoni, M., Clennell, M. B., McNamara, D. D., Nole, M., Wang, X., et al. (2020). Physical properties and gas hydrate at a near-seafloor thrust fault, Hikurangi Margin, New Zealand. *Geophysical Research Letters*, *47*(16), e2020GL088474. https://doi.org/10.1029/2020gl088474

Darby, D., & Funnell, R. H. (2001). Overpressure associated with a convergent plate margin: East Coast Basin, New Zealand. *Petroleum Geoscience*, *7*(3), 291–299. https://doi.org/10.1144/petgeo.7.3.291

Davis, E. E., Villinger, H., & Sun, T. (2015). Slow and delayed deformation and uplift of the outermost subduction prism following ETS and seismogenic slip events beneath Nicoya Peninsula, Costa Rica. *Earth and Planetary Science Letters*, *410*, 117–127. https://doi.org/10.1016/j.epsl.2014.11.015

Dimitrova, L., Wallace, L., Haines, A., & Williams, C. (2016). High-resolution view of active tectonic deformation along the Hikurangi subduction margin and the Taupo Volcanic Zone, New Zealand. *New Zealand Journal of Geology and Geophysics*, *59*(1), 43–57. https://doi.org/10.1080/00288306.2015.1127823

Dixon, T. H., Jiang, Y., Malservisi, R., McCaffrey, R., Voss, N., Protti, M., & Gonzalez, V. (2014). Earthquake and tsunami forecasts: Relation of slow slip events to subsequent earthquake rupture. *Proceedings of the National Academy of Sciences of the United States of America*, *111*(48), 17039–17044. https://doi.org/10.1073/pnas.1412299111

Doser, D. I., & Webb, T. H. (2003). Source parameters of large historical (1917–1961) earthquakes, North Island, New Zealand. *Geophysical Journal International*, *152*(3), 795–832. https://doi.org/10.1046/j.1365-246x.2003.01895.x

Duan, B. (2010). Role of initial stress rotations in rupture dynamics and ground motion: A case study with implications for the Wenchuan earthquake. *Journal of Geophysical Research*, *115*, B05301. https://doi.org/10.1029/2009jb006750

Fagereng, A., Savage, H. M., Morgan, J. K., Wang, M., Meneghini, F., Barnes, P. M., et al. (2019). Mixed deformation styles observed on a shallow subduction thrust, Hikurangi margin, New Zealand. *Geology*, *47*(9), 872–876. https://doi.org/10.1130/g46367.1

Greve, A., Kars, M., Zerbst, L., Stipp, M., & Hashimoto, Y. (2020). Strain partitioning across a subduction thrust fault near the deformation front of the Hikurangi subduction margin, New Zealand: A magnetic fabric study on IODP Expedition 375 Site U1518. *Earth and Planetary Science Letters*, *542*, 116322. https://doi.org/10.1016/j.epsl.2020.116322

Haines, A. J., & Wallace, L. M. (2020). New Zealand-wide geodetic strain rates using a physics-based approach. *Geophysical Research Letters*, *47*(1), e2019GL084606. https://doi.org/10.1029/2019gl084606

Hardebeck, J. L., & Okada, T. (2018). Temporal stress changes caused by earthquakes: A review. *Journal of Geophysical Research: Solid Earth*, *123*(2), 1350–1365. https://doi.org/10.1002/2017jb014617

Heidbach, D. O. (2016). *WSM quality ranking scheme, database description and analysis guidelines for stress indicator*. WSM Technical Report 16-01.

Hirose, H., Hirahara, K., Kimata, F., Fujii, N., & Miyazaki, S. (1999). A slow thrust slip event following the two 1996 Hyuganada Earthquakes beneath the Bungo Channel, southwest Japan. *Geophysical Research Letters*, *26*(21), 3237–3240. https://doi.org/10.1029/1999gl010999

Huffman, K. A., Saffer, D. M., & Dugan, B. (2016). In situ stress magnitude and rock strength in the Nankai accretionary complex: A novel approach using paired constraints from downhole data in two wells. *Earth, Planets and Space*, *68*(1), 1–9. https://doi.org/10.1186/s40623-016-0491-4

Ikari, M. J., Wallace, L. M., Rabinowitz, H. S., Savage, H. M., Hamling, I. J., & Kopf, A. J. (2020). Observations of laboratory and natural slow slip events: Hikurangi Subduction Zone, New Zealand. *Geochemistry, Geophysics, Geosystems*, *21*(2), e2019GC008717. https://doi.org/10.1029/2019gc008717

Ito, T., & Zoback, M. D. (2000). Fracture permeability and in situ stress to 7 km depth in the KTB scientific drillhole. *Geophysical Research Letters*, *27*(7), 1045–1048. https://doi.org/10.1029/1999gl011068

Langridge, R. M., Ries, W. F., Litchfield, N. J., Villamor, P., Dissen, R. J. V., Barrell, D., et al (2016). The New Zealand Active Faults Database. *New Zealand Journal of Geology and Geophysics*, *59*(1), 86–96. https://doi.org/10.1080/00288306.2015.1112818

Lawrence, M. J. F. (2018). Structural and sedimentological *i*nterpretation of well *d*ata from the Wairoa area, North Island, New Zealand. GNS Science Report No. 2018/28. Retrieved from https://shop.gns.cri.nz/account.php?action=download_item&data=MTI2NjUsN-DE5Miw3Njk2LDZjMjE5OTA3MjIxOTAxN2Y1ZjBkZDVkM2Q1YTA2M2VmLDQyMTQxMzE2ODgwNDgxMDM5NDM3MjIzNjk-wNTM1OTI4ODE0

Lin, W., Byrne, T. B., Kinoshita, M., McNeill, L. C., Chang, C., Lewis, J. C., et al. (2015). Distribution of stress state in the Nankai subduction zone, southwest Japan and a comparison with Japan Trench. *Tectonophysics*, *692*, 1–12. https://doi.org/10.1016/j.tecto.2015.05.008

Lin, W., Conin, M., Moore, J. C., Chester, F. M., Nakamura, Y., Mori, J. J., et al. (2013). Stress state in the largest displacement area of the 2011 Tohoku-Oki earthquake. *Science*, *339*(6120), 687–690. https://doi.org/10.1126/science.1229379

Lin, W., Yeh, E.-C., Hung, J.-H., Haimson, B., & Hirono, T. (2009). Localized rotation of principal stress around faults and fractures determined from borehole breakouts in hole B of the Taiwan Chelungpu-fault Drilling Project (TCDP). *Tectonophysics*, *482*(1), 82–91. https://doi.org/10.1016/j.tecto.2009.06.020

Magee, M. E., & Zoback, M. D. (1993). Evidence for a weak interplate thrust fault along the northern Japan subduction zone and implications for the mechanics of thrust faulting and fluid expulsion. *Geology*, *21*(9), 809. https://doi.org/10.1130/0091-7613(1993)021<0809:efawit>2.3.co;2

Mardia, K. V. (1975). Statistics of directional data. *Journal of the Royal Statistical Society: Series B (Methodological)*, *37*(3), 349–371. https://doi.org/10.1111/j.2517-6161.1975.tb01550.x

McNamara, D. D., Massiot, C., & Lewis, B. (2015). Heterogeneity of structure and stress in the Rotokawa Geothermal Field, New Zealand. *Journal of Geophysical Research: Solid Earth*, *120*(2), 1243–1262. https://doi.org/10.1002/(issn)2169-9356

McNamara, D. D., Milicich, S. D., Massiot, C., Villamor, P., McLean, K., Sepulveda, F., & Ries, W. F. (2019). Tectonic controls on Taupo Volcanic Zone geothermal expression: Insights from Te Mihi, Wairakei Geothermal Field. *Tectonics*, *147*(1), 71–23. https://doi.org/10.1029/2018tc005296

Miller, D. J., & Dunne, T. (1996). Topographic perturbations of regional stresses and consequent bedrock fracturing. *Journal of Geophysical Research*, *101*(B11), 25523–25536. https://doi.org/10.1029/96jb02531

Mountjoy, J. J., & Barnes, P. M. (2011). Active upper plate thrust faulting in regions of low plate interface coupling, repeated slow slip events, and coastal uplift: Example from the Hikurangi Margin, New Zealand. *Geochemistry*, *12*(1), Q01005. https://doi.org/10.1029/2010gc003326

Obara, K., Hirose, H., Yamamizu, F., & Kasahara, K. (2004). Episodic slow slip events accompanied by non-volcanic tremors in southwest Japan subduction zone. *Geophysical Research Letters*, *31*, L23602. https://doi.org/10.1029/2004gl020848

Pecher, I. A., Barnes, P. M., LeVay, L. J., & the Expedition 372A Scientists. (2019). Creeping gas hydrate slides. In *Proceedings of the International Ocean Discovery Program, 372A. International Ocean Discovery Program*. https://doi.org/10.14379/iodp.proc.372a.2019

Pedley, K. L., Barnes, P. M., Pettinga, J. R., & Lewis, K. B. (2010). Seafloor structural geomorphic evolution of the accretionary frontal wedge in response to seamount subduction, Poverty Indentation, New Zealand. *Marine Geology*, *270*(1–4), 119–138. https://doi.org/10.1016/j.margeo.2009.11.006

Saffer, D. M., Wallace, L. M., Barnes, P. M., Pecher, I. A., Petronotis, K. E., LeVay, L. J., et al. (2019). *Proceedings of the International Ocean Discovery Program Site U1518*. Undefined. https://doi.org/10.14379/iodp.proc.372b375.103.2019

Sibson, R., Ghisetti, F., & Ristau, J. (2011). Stress control of an evolving strike-slip fault system during the 2010–2011 Canterbury, New Zealand, earthquake sequence. *Seismological Research Letters*, *82*(6), 824–832. https://doi.org/10.1785/gssrl.82.6.824

Song, I., Saffer, D. M., & Flemings, P. B. (2011). Mechanical characterization of slope sediments: Constraints on in situ stress and pore pressure near the tip of the megasplay fault in the Nankai accretionary complex. *Geochemistry, Geophysics, Geosystems*, *12*, Q0AD17. https://doi.org/10.1029/2011gc003556

Sun, T., Saffer, D., & Ellis, S. (2020). Mechanical and hydrological effects of seamount subduction on megathrust stress and slip. *Nature Geoscience*, *13*(3), 249–255. https://doi.org/10.1038/s41561-020-0542-0

Tingay, M., Reinecker, J., & Müller, B. (2008). *Borehole breakout and drilling-induced fracture analysis from image logs*. World Stress Map Project.

Townend, J., Sherburn, S., Arnold, R., Boese, C., & Woods, L. (2012). Three-dimensional variations in present-day tectonic stress along the Australia-Pacific plate boundary in New Zealand. *Earth and Planetary Science Letters*, *353*, 47–59. https://doi.org/10.1016/j.epsl.2012.08.003

Wallace, L. M., Beavan, J., Bannister, S., & Williams, C. (2012). Simultaneous long-term and short-term slow slip events at the Hikurangi subduction margin, New Zealand: Implications for processes that control slow slip event occurrence, duration, and migration. *Journal of Geophysical Research*, *117*, B11402. https://doi.org/10.1029/2012jb009489

Wallace, L. M., Beavan, J., McCaffrey, R., & Darby, D. (2004). Subduction zone coupling and tectonic block rotations in the North Island, New Zealand. *Journal of Geophysical Research*, *109*(B), B12406. https://doi.org/10.1029/2004jb003241

Wallace, L. M., & Eberhart-Phillips, D. (2013). Newly observed, deep slow slip events at the central Hikurangi margin, New Zealand: Implications for downdip variability of slow slip and tremor, and relationship to seismic structure. *Geophysical Research Letters*, *40*(20), 5393–5398. https://doi.org/10.1002/2013gl057682

Wallace, L. M., Fagereng, Å., & Ellis, S. (2012). Upper plate tectonic stress state may influence interseismic coupling on subduction megathrusts. *Geology*, *40*(10), 895–898. https://doi.org/10.1130/g33373.1

Wallace, L. M., Saffer, D. M., Barnes, P. M., Pecher, I. A., Petronotis, K. E., LeVay, L. J., et al. (2019a). *Proceedings of the International Ocean Discovery Program - Expedition 372B/375 Methods*. Undefined. https://doi.org/10.14379/iodp.proc.372b375.102.2019

Wallace, L. M., Saffer, D. M., Barnes, P. M., Pecher, I. A., Petronotis, K. E., LeVay, L. J., et al. (2019b). *Proceedings of the International Ocean Discovery Program - Expedition 372B/375 Summary*. Undefined. https://doi.org/10.14379/iodp.proc.372b375.101.2019.

Wallace, L. M., Wallace, J. B. L. M., & Beavan, J. (2010). Diverse slow slip behavior at the Hikurangi subduction margin, New Zealand. *Journal of Geophysical Research*, *115*(B), B12402. https://doi.org/10.1029/2010jb007717

Wallace, L. M., Webb, S. C., Ito, Y., Mochizuki, K., Hino, R., Henrys, S., et al. (2016). Slow slip near the trench at the Hikurangi subduction zone, New Zealand. *Science*, *352*(6286), 701–704. https://doi.org/10.1126/science.aaf2349

Warren-Smith, E., Fry, B., Wallace, L., Chon, E., Henrys, S., Sheehan, A., et al. (2019). Episodic stress and fluid pressure cycling in subducting oceanic crust during slow slip. *Nature Geoscience*, *12*(6), 475–481. https://doi.org/10.1038/s41561-019-0367-x

Williams, C. A., Eberhart-Phillips, D., Bannister, S., Barker, D. H. N., Henrys, S., Reyners, M., & Sutherland, R. (2013). Revised interface geometry for the Hikurangi Subduction Zone, New Zealand. *Seismological Research Letters*, *84*(6), 1066–1073. https://doi.org/10.1785/0220130035

Zal, H. J., Jacobs, K., Savage, M. K., Yarce, J., Mroczek, S., Graham, K., et al. (2020). Temporal and spatial variations in seismic anisotropy and Vp/Vs ratios in a region of slow slip. *Earth and Planetary Science Letters*, *532*, 115970. https://doi.org/10.1016/j.epsl.2019.115970

Zoback, M. D., & Townend, J. (2001). Implications of hydrostatic pore pressures and high crustal strength for the deformation of intraplate lithosphere. *Tectonophysics*, *336*(1–4), 19–30. https://doi.org/10.1016/s0040-1951(01)00091-9

Zoback, M. L., Zoback, M. D., Adams, J., Assumpção, M., Bell, S., Bergman, E. A., et al. (1989). Global patterns of tectonic stress. *Nature*, *341*(6240), 291–298. https://doi.org/10.1038/341291a0